

A Sub-solar Fe/O, $\log(T/K) \sim 7.5$ Gas Component Permeating the Milky Way's CGM

Armando Lara-DI,¹ Yair Krongold,¹ Smita Mathur,^{2,3} Sanskriti Das,⁴ Anjali Gupta,² O. Segura Montero,¹

¹*Instituto de Astronomía, Universidad Nacional Autónoma de México, 04510 Mexico City, Mexico*

²*Astronomy Department, The Ohio State University, Columbus, OH 43210*

³*Center for Cosmology and Astro-Particle Physics, The Ohio State University, Columbus, OH 43220*

⁴*Kavli Institute for Particle Astrophysics & Cosmology, Stanford University, 452 Lomita Mall, Stanford, CA 94305, USA*

Accepted XXX. Received YYY; in original form ZZZ

ABSTRACT

Our study focuses on characterizing the highly ionized gas within the Milky Way's (MW) Circumgalactic Medium (CGM) that gives rise to ionic transitions in the X-ray band 2 - 25 Å. Utilizing stacked Chandra/ACIS-S MEG and LETG spectra toward QSO sightlines, we employ the self-consistent hybrid ionization code PHASE to model our data. The stacked spectra are optimally described by three distinct gas phase components: a warm ($\log(T/K) \sim 5.5$), warm-hot ($\log(T/K) \sim 6$), and hot ($\log(T/K) \sim 7.5$) components. These findings confirm the presence of the hot component in the MW's CGM indicating its coexistence with a warm and a warm-hot gas phases. We find this hot component to be homogeneous in temperature but inhomogeneous in column density. The gas in the hot component requires over-abundances relative to solar to be consistent with the Dispersion Measure (DM) from the Galactic halo reported in the literature. For the hot phase we estimated a $DM = 55.1^{+29.9}_{-23.7}$ pc cm⁻³. We conclude that this phase is either enriched in Oxygen, Silicon, and Sulfur, or has metallicity over 6 times solar value, or a combination of both. We do not detect Fe L-shell absorption lines, implying $O/Fe \geq 4$. The non-solar abundance ratios found in the super-virial gas component in the Galactic halo suggest that this phase arises from Galactic feedback.

Key words: Galaxy: halo – Galaxy: structure – X-rays: general

1 INTRODUCTION

The circumgalactic medium (CGM) refers to the gaseous component located beyond the galactic disc and within the galactic virial radius. The CGM is a mixed medium with complex structures like filaments, bubbles, and multiphase regions. It comprises ionized and neutral gas with different temperatures and densities (e.g., Tumlinson et al. 2017; Mathur 2022).

The CGM is thought to play a crucial role in regulating the exchange of matter and energy between the galactic disc and its environment (e.g., Kereš et al. 2005, Zheng et al. 2015). Numerical simulations have shown that shock-heating processes might have heated and ionized the gas during galaxy formation, preventing it from falling into the galactic disc. On the other hand, feedback processes such as supernovas and galactic winds could have expelled large amounts of material into the CGM (e.g., Stinson et al. 2012). Processes such as the infall of material (commonly pristine gas) from the intergalactic medium towards the galactic disc and the expulsion of metals formed in stars from the disc into the surrounding region make the CGM an important clue to understanding galactic formation and evolution (e.g., Tumlinson et al. 2017; Li et al. 2018). These studies suggest that the CGM is a large reservoir of gas that can fuel future star formation within the galaxy and the place where the missing baryons and metals could reside.

In the local universe, at galactic scales, the number of baryons observed in galaxies with luminosity less or near Schechter L^* lies

near half under the amount of baryonic mass predicted by the nucleosynthesis in the Big Bang theory and inferred from the density fluctuations of the cosmic microwave background. For galaxies less massive, more mass is missing (e.g., Kirkman et al. 2003 and references therein; Planck Collaboration et al. 2016, McGaugh et al. 2010). Coupled with the Missing Baryon Problem, there is also The Missing Metal Problem at galactic scales. The number of metals expected from the stars observed and the star formation history of galaxies is about two times larger than the number of metals we can observe (Peeples et al. 2014).

Theoretical studies suggest that the missing baryons and missing metals in galaxies might reside in the CGM; however, its diffuse nature makes it difficult to study this material (e.g., Feldmann et al. 2013; Mathur et al. 2021; Mathur et al. 2023).

Because of our unique point of reference, studying the CGM of the Milky Way is much easier than studying it in external galaxies. A common way to detect the CGM of the Milky Way is by studying it in absorption against bright background sources, such as quasars (e.g., Gupta et al. 2012, Mathur 2022).

The CGM is expected to be close to the galaxy's virial temperature. For a Milky Way-like galaxy, this temperature is about $\log(T/K) \sim 6$. We will call the gas at this high temperature the warm-hot component. For the Milky Way, this gas phase has been studied in emission and absorption using UV and X-ray spectra (e.g., Wang et al. 2005; Gupta et al. 2012; Das et al. 2019a).

Gupta et al. (2012) detected in absorption towards extragalactic

sight lines O_{VII} and O_{VIII} at $z = 0$. Using and combining their results with emission results from [Henley et al. 2010](#), they derive that the warm-hot phase of the Milky Way CGM is a massive component of about $\log(M/M_{\odot}) \sim 10$, which extends over a vast region around the galactic disc. Their results suggest that it is in this component where the missing baryons and metals could reside.

In recent studies, [Das et al. \(2019a\)](#), [Das et al. \(2021b\)](#), and detected a hotter gas component in the Milky Way CGM for the first time. They found a gas phase with super-virial temperature at $\log(T/\text{K}) \gtrsim 7$. Hereafter, we will refer to this component as hot. Using deep XMM-Newton RGS observations of the blazar 1ES 1553+113, [Das et al. \(2019a\)](#) detected in absorption $\text{Ne X } K\alpha$ associated with this hot component. Later on, in 2021 [Das et al. \(2021b\)](#) also found $\text{Si XIV } K\alpha$ and $\text{Ne X } K\alpha$ in the line of sight towards the blazar Mkn 421. Their results in these two lines of sight indicate that the CGM is a multiphase system with a warm ($\log(T/\text{K}) \sim 5.5$), warm-hot ($\log(T/\text{K}) \sim 6$), and hot ($\log(T/\text{K}) \sim 7.5$) components.

Focused on these gas components, and using Chandra observations towards 47 different sightlines and the stacking technique, [Lara-DI et al. \(2023\)](#) (hereafter LDI-2023a) were able to detect $\text{Si XIV } K\alpha$ and for the first time $\text{S XV I } K\alpha$ at $z = 0$ in absorption. Their discovery confirms the presence of a hot component in the Milky Way CGM, suggesting it is a widespread component throughout the entire CGM. The presence of the hot component was also confirmed by [McClain et al. \(2024\)](#) in the sightline toward NGC 3783.

The newly discovered hot component was also detected in emission (e.g., [Das et al. 2019b](#); [Bluem et al. 2022](#); [Gupta et al. 2021](#); [Bhattacharyya et al. 2023](#); [Gupta et al. 2023](#)). [Bhattacharyya et al. \(2023\)](#) studied in emission the hot phase of the CGM around the Mkn 421 sightline. Their study complements the work done by [Das et al. \(2021b\)](#) in the line of sight towards Mkn 421, showing that the emitting gas has higher density, possibly coming from regions close to the Galactic disc. On the other hand, the absorption measurements arise from low densities extending to the virial radius. They found a scatter in the temperature in both the warm-hot component and the hot component; this contributes to understanding the CGM as a multiphase system.

Despite these recent efforts, characterizing the CGM remains challenging. Information about its geometry, homogeneity, and how the different gas phases expand through the entire CGM Milky Way remains to be determined. The super-virial hot component is not expected from theoretical studies, and its finding opens new questions crucial to better understanding galactic formation and evolution.

This paper focuses on absorption studies of the Milky Way CGM. We use the LDI-2023a data sample to characterize the CGM by identifying the gas phases from which these and other absorption lines come. LDI-2023a focused on the spectral range 4 - 8 Å; now, we will focus on the study of the spectral range from 2 to 25 Å using a self-consistent ionization model (PHASE, [Krongold et al. 2003](#)) to fit the data. We structure our paper as follows. In Section 2, we present the sample selection. In Section 3, we describe the data analysis. In Section 4, we show our results, and in Section 5, we discuss their implications.

2 DATA SAMPLE

This paper uses the same data sample and stacked spectra used in LDI-2023a. The data sample consists of 47 different sight lines to QSOs, Seyfert-1, and Blazars from Chandra X-ray Observatory public observations. This sample excludes changing look Active Galactic

Nuclei (AGN)¹, which sometimes act like a Seyfert-1 and sometimes as Syfert-2 objects. We also exclude long observations with very high S/N² that would dominate the stacked spectra in our analysis, along with ES1553+113 and Mkn 421 sightlines used by [Das et al. \(2019a\)](#) and [Das et al. \(2021b\)](#). Finally, NGC 4051 ($z = 0.002$), which presents at $z = 0$ clear contribution of narrow absorption lines due to its Warm Absorber (WA), was also excluded (e.g., [Krongold et al. 2007](#)). In this way, we avoid intrinsic absorption lines of the WA contaminating our analysis. The sightlines chosen have high Galactic latitude, meaning our data has a small cross-section with the Milky Way's Interstellar Medium (ISM) (see LDI-2023a for more details).

The stacked spectra with MEG observations comprise 46 (10.96 Ms) of the 47 sightlines, while LETG has nine (1.09 Ms). Except for one sightline (TON S 180), all the sightlines covered by LETG are contained within MEG. The contribution of LETG sightlines to the overall exposure time of MEG amounts to about 10%. It is important to note that MEG data is dominated by sources with WA, whereas LETG is not.

We study the spectral range 2 - 25 Å, with a signal-to-noise (S/N) ratio of 2181 for MEG and 651 for LETG. In LDI-2023a, the complete list of sightlines, the Aitoff projection of these targets, and the complete table with the list of individual observations are included. See also LDI-2023a for details on how the data was reprocessed and stacked.

3 ANALYSIS

3.1 Fitting the Continuum

To analyze MEG and LETG stacked spectra, we used the spectral fitting software XSPEC (v12.13.0) with χ^2 statistics. Errors presented in this paper correspond to 1σ level.

We first modeled the continuum of each spectrum from 2.0 to 25.0 Å. We used a model comprising a power law (powerlaw), a black body (bbody) component, an ISM absorption component (Tbabs), and as many Gaussian lines (agauss) as required to account for AGN intrinsic absorption or emission features (i.e., lines produced intrinsically in the sources and not arising from the Milky Way's CGM).

3.2 PHASE

To model the absorption lines on the spectra arising from the gas components at $z = 0$ of the Milky's Way CGM, we used the hybrid (photo + collision) ionization code PHASE ([Krongold et al. 2003](#)). This code allows the analysis of X-ray spectra by generating a synthetic spectrum that fits the data and gives the gas phase component that best describes it. PHASE has as free parameters the temperature of the gas (T), the hydrogen column density (N_H), the redshift (z), the micro-turbulent velocity of the gas (v), the ionization parameter (U), and the abundances of the elements, which are set to solar by default.

The CGM is expected to have densities for which photoionization from the metagalactic background should be negligible. Therefore, in spectroscopic modeling we fixed the ionization parameter of the gas to low values ($\log U \sim -4$). Since our study focuses on the Milky Way's CGM, we set the redshift $z \approx 0$. The width of the lines was set to be less than the resolution element of the instrument. Therefore,

¹ Mkn 590

² 3C 273 and PKS 2155-304

our model is constrained to fit narrow lines. In particular, $v \approx 10$ km s⁻¹.

This way, we added a PHASE component to the continuum model. This first component was set to fit the virial component (warm-hot) by only considering spectral ranges where Ne_{IX} and O_{VII} appear and letting fit the model to the best log(T/K) and log(N_H/cm^{-2}) for this component. Once we had the best temperature for this component, we extended our analysis to cover all spectral ranges and introduced an additional hotter component (hot) with a higher temperature. Finally, we included a warmer (warm) component with a lower temperature and fitted the three components simultaneously. However, it is important to note that our results do not depend on the order in which the PHASE components are added to the continuum.

The final statistic for the model fitting the continuum on MEG was $\chi^2/d.o.f = 6600.48/4599$, and $\chi^2/d.o.f = 1606.56/1837$ on LETG.

3.2.1 Abundances

In the X-ray band, we do not have a diagnostic for Hydrogen, so we cannot constrain the absolute metallicity of the CGM. However, we can study the relative abundances of different elements. To do this, we allow each element's abundance to vary independently when necessary.

4 RESULTS

Figures 1 and 2 show the lines fitted with PHASE. The best model fitting MEG and LETG data comprises three different gas components. Each component models different absorption lines in the rest frame of the Milky Way. According to our models, some ionic transitions span through two different temperature components, while others are produced in a single gas phase.

In Table 2, we present the physical parameters of the three components modeled in MEG and LETG datasets. We display the position of the absorption line, its Equivalent Width (EW) and its Ionic Column Density (N_{ion}). Next to Si_{XIV} $K\alpha$ and S_{XVI} $K\alpha$ parameters in the hot component, we also included in columns (12) and (14) the EW and the ionic column density of the lines as reported in LDI-2023a.

4.1 ACIS-S HETG-MEG

The first component modeling MEG data is a warm-hot component at log(T/K) = $6.19^{+0.06}_{-0.08}$ and column density log(N_H/cm^{-2}) = $19.12^{+0.08}_{-0.10}$ (hereafter MEG-WARM-HOT). The absorption lines modeled with this component are N_{VI} $K\beta$, N_{VII} $K\alpha$, Ne_{IX} $K\alpha$, O_{VII} $K\alpha$, O_{VII} $K\beta$, O_{VII} $K\gamma$, and O_{VIII} $K\alpha$. This component improves the fit by a $\Delta\chi^2$ of 61 for two free parameters.

The second component is a hot component at log(T/K) = 7.50 ± 0.03 and column density log(N_H/cm^{-2}) = $21.30^{+0.05}_{-0.06}$ (hereafter MEG-HOT). The absorption lines modeled with this component are O_{VIII} $K\alpha$, Si_{XIV} $K\alpha$, and S_{XVI} $K\alpha$. This component improves the fit by a $\Delta\chi^2$ of 57 for two additional free parameters.

The third component comprising the model fitting MEG data is a warm component at log(T/K) = $5.39^{+0.13}_{-0.07}$ and column density log(N_H/cm^{-2}) = $18.08^{+0.31}_{-0.40}$ (hereafter MEG-WARM). Only N_{VI} $K\beta$ absorption line is modeled with this component improving the fit marginally by a $\Delta\chi^2$ of 2 for two additional free parameters, see Table 1.

N_{VI} $K\beta$ contributes on the warm and warm-hot component,

while O_{VIII} $K\alpha$ is contributing in the warm-hot and hot components. On the other hand, N_{VII} $K\alpha$, Ne_{IX} $K\alpha$, O_{VII} $K\alpha$, O_{VII} $K\beta$, O_{VII} $K\gamma$ contribute exclusively to the warm-hot component. Si_{XIV} and S_{XVI} contribute exclusively to the hot component.

4.2 ACIS-S LETG

The best model fitting LETG data comprises three distinct gas components. The first component (hereafter LETG-WARM-HOT) represents a warm-hot component with a temperature of log(T/K) = 6.56 ± 0.12 and a column density of log(N_H/cm^{-2}) = $19.56^{+0.21}_{-0.27}$. This component models Ne_{IX} $K\alpha$, O_{VII} $K\alpha$, and O_{VIII} $K\alpha$ absorption lines. This component improves the fit only by a $\Delta\chi^2$ of 10 for two additional free parameters.

The second and hotter component modeling LETG data is a gas component with a temperature log(T/K) = 7.50 ± 0.05 and a column density of log(N_H/cm^{-2}) = $21.75^{+0.08}_{-0.14}$. This component is referred here as LETG-HOT. The absorption lines modeled with this component are O_{VIII} $K\alpha$, S_{XVI} $K\alpha$, and Si_{XIV} $K\alpha$. This component improves the fit by a $\Delta\chi^2$ of 31 for two additional free parameters.

Finally, the third component fitting this dataset is characterized by a temperature of log(T/K) = 5.64 ± 0.06 and a column density of log(N_H/cm^{-2}) = $19.76^{+0.09}_{-0.11}$, (hereafter LETG-WARM). The absorption lines modeled in this component are O_{VI} $K\alpha$ and O_{VII} $K\alpha$. This component improves the fit by a $\Delta\chi^2$ of 36 for two additional free parameters, see Table 1.

In our results for the LETG data, we find O_{VI} $K\alpha$ contributing exclusively to LETG-WARM. O_{VII} is present in the LETG-WARM and LETG-WARM-HOT components. Ne_{IX} is found exclusively in the LETG-WARM-HOT component. O_{VIII} contributes in both, LETG-WARM-HOT and LETG-HOT, while Si_{XIV} and S_{XVI} are exclusively found in LETG-HOT.

4.3 Metallicity of the CGM

In MEG data, we could not model MEG-HOT with solar Fe abundance since it grossly overpredicts the Fe absorption lines. In Figure 3, we present the spectrum of MEG data in the range 10.4 - 11.2 Å. In this Figure, we show how the model overpredicts the absorption lines of Fe when its abundance is that of Oxygen. To avoid this, the model must consider an abundance of Fe at least four times less than that of Oxygen. We find the abundance of other elements correspond to solar mixture.

In LETG data, the model also overpredicts the Fe L-shell lines in the hot component. Figure 3 shows how the model overpredicts Fe when its abundance is that of Oxygen. In this case, the abundance of Fe in the hot component needs to be at least six times less than that of Oxygen to properly model the data.

We also noticed that for LETG the code prefers ~ 4 times more S/O than the solar value. In this same dataset, the code prefers ~ 1.5 times solar Si/O. Nonetheless, the data is not very sensitive to the abundance of these two elements.

5 DISCUSSION

We have found that the Milky Way's CGM comprises at least three phases, a warm (log(T/K) ~ 5.5), warm-hot (log(T/K) ~ 6), and hot (log(T/K) ~ 7.5) component, confirming previous results pointing to the third phase with high temperature (Das et al. 2019 and 2021; LDI-2023a). This hot phase has a column density at least an order of magnitude higher than the warm-hot and warm

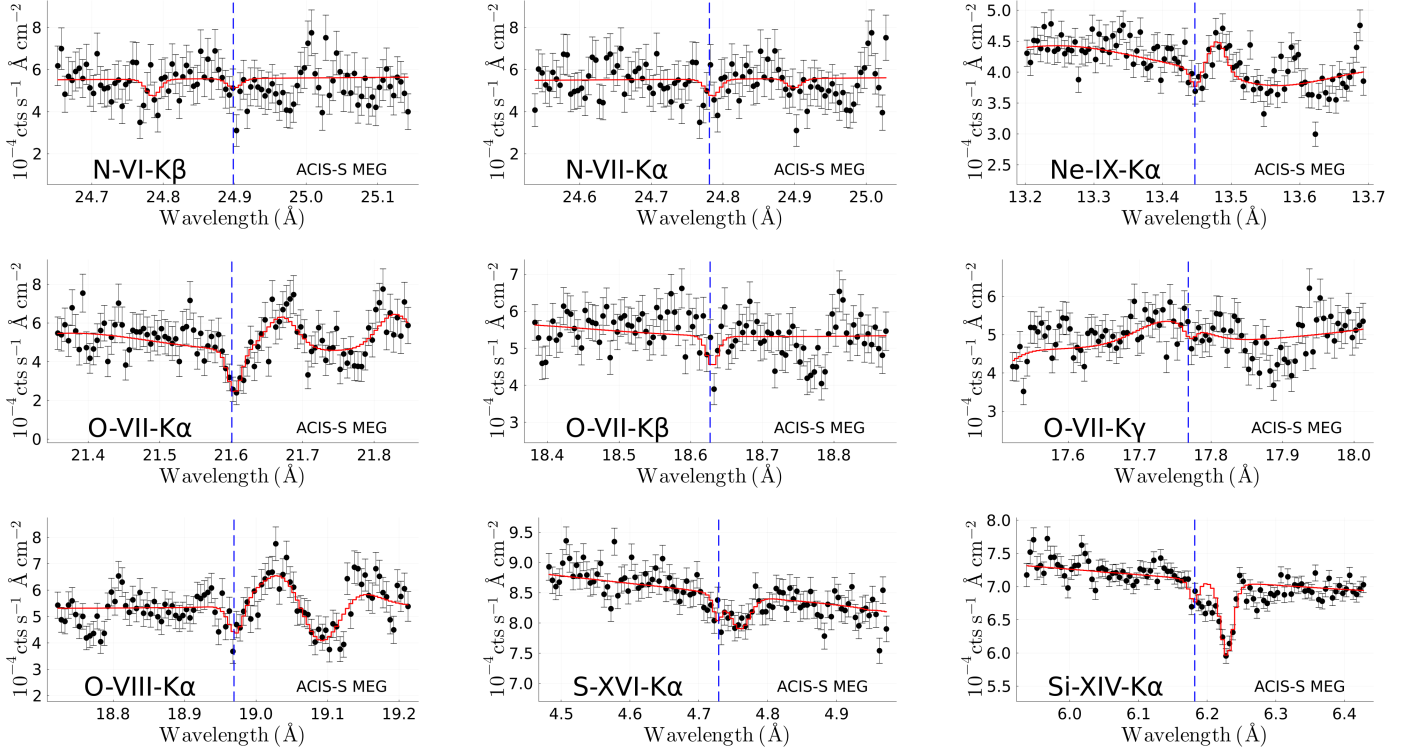


Figure 1. We present the plots of absorption lines for different ionic transitions in MEG data modeled with PHASE. The data points are represented by black markers, the best-fit model is indicated by a red line, and the position of the theoretical rest wavelength is denoted by a vertical blue dashed line.

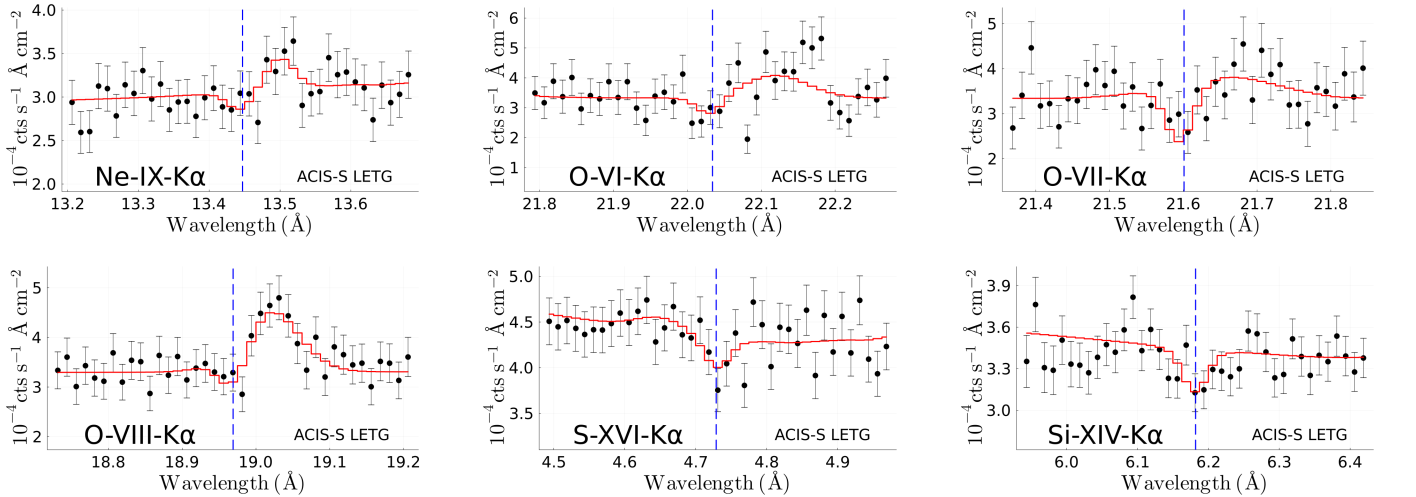


Figure 2. We present the plots of absorption lines for different ionic transitions in LETG data modeled with PHASE. The data points are represented by black markers, the best-fit model is indicated by a red line, and the position of the theoretical rest wavelength is denoted by a vertical blue dashed line.

components. This result is consistent in MEG and LETG data and previous detections of the hot phase (Das et al. 2019 and 2021; LDI-2023a).

5.1 Physical state of the gas in the hot component

It is interesting to note that we do not see $\text{Ne}_X \text{K}\alpha$ in MEG or LETG. This is consistent with the high temperature of the hot component. Ne_X peaks around $\log(T/\text{K}) \sim 6.7$, and the fraction of Ne_X decreases

sharply for higher temperatures. At $\log(T/\text{K}) \sim 7.5$, Ne is almost completely ionized. Therefore, our data is consistent with not being able to detect Ne_X in MEG or LETG, and this is a nice confirmation that the temperature of the gas reaches $\log(T/\text{K}) \sim 7.5$. The Ne_X line should be very weak due to the plasma being very hot. Therefore, it is not detectable with the S/N of our data. In Figure 4 we show our model fitting the data at the position of the rest-wavelength of Ne_X . We see no prominent absorption line of this ion. Das et al. (2019a) and Das et al. (2021b) reported the detection of this line at the same

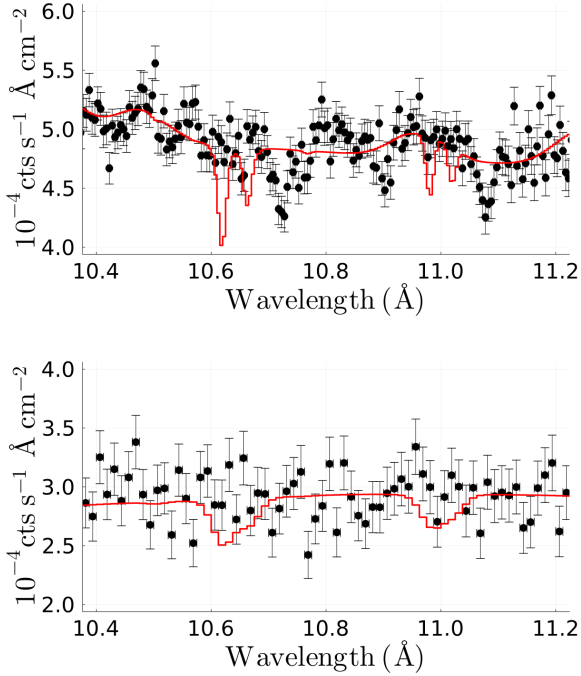


Figure 3. These plots present the model in red overpredicting Fe L-shell absorption lines in MEG (top) and LETG (bottom) data when Fe abundance is set to be that of Oxygen.

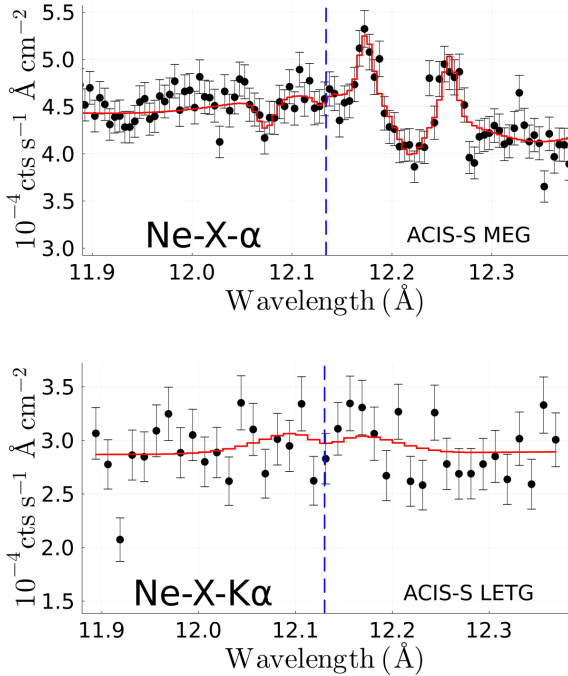


Figure 4. Here we present a spectral window of our MEG (top) and LETG (bottom) data modeled. We show in vertical blue line the position of Ne $K\alpha$ res-wavelength

Table 1. $\Delta\chi^2$ improved in MEG and LETG when including a component modeling a different gas phase with two free parameters.

Component	$\log(T/K)$	$\log(N_H/\text{cm}^{-2})$	$\Delta\chi^2$
MEG-WARM	$5.39^{+0.13}_{-0.07}$	$18.08^{+0.31}_{-0.40}$	2
MEG-WARM-HOT	$6.19^{+0.06}_{-0.08}$	$19.12^{+0.08}_{-0.10}$	61
MEG-HOT	7.50 ± 0.03	$21.30^{+0.05}_{-0.06}$	57
LETG-WARM	5.64 ± 0.06	$19.76^{+0.09}_{-0.11}$	36
LETG-WARM-HOT	6.56 ± 0.12	$19.56^{+0.21}_{-0.27}$	10
LETG-HOT	7.50 ± 0.05	$21.75^{+0.08}_{-0.14}$	31

temperature, but their model required super-solar Ne/O abundance. If the plasma had been a factor of two or three lower temperature, say at $\log(T/K) \sim 7$, the Ne X line should be very prominent and detectable in our spectra. This result excludes the presence of high quantities of gas in the CGM with temperatures $\log(T/K)$ over ~ 6.5 and below ~ 7.5 in the sightlines probed in the stacked spectra.

5.2 Comparison between detections of LDI-2023a and this work

As mentioned in § 1, LDI-2023a clearly detected Si XIV $K\alpha$ and S XV $K\alpha$ in the same stacked spectra presented here. In Table 2, we show the EW and N_{ion} predicted by our model with PHASE, contrasted with those measured empirically by LDI-2023a over MEG and LETG with Gaussians. The striking similarity in these values shows that detecting these elements is a robust result in these studies. Therefore, the results presented here fully confirm, with a self-consistent ionization model, the presence of a hot super-virial gas component in the Milky Way’s CGM.

5.3 Statistical significance of each component

In Table 1, we show how much each component changes the χ^2 statistic for two free parameters (namely, the temperature and the column density of the gas). For MEG data, we find that the gas components weighting more in the statistic are MEG-WARM-HOT with $\Delta\chi^2 = 61$ and MEG-HOT with $\Delta\chi^2 = 57$. The fact that these phases are statistically significant is not a surprise, given the number of absorption lines fit with MEG-WARM-HOT component and given the high column density of MEG-HOT component. On the other hand, the MEG-WARM only changes the statistic by a $\Delta\chi^2 = 2$. We note, however, that there is vast evidence of the presence of this component in UV data (e.g., Tumlinson et al. 2017 and references therein).

In LETG we find that the LETG-WARM and LETG-HOT weight similarly with $\Delta\chi^2 = 36$ and $\Delta\chi^2 = 31$ respectively, making both components statistically significant. On the other hand, LETG-WARM-HOT component only weights $\Delta\chi^2 = 10$ in our model, making it barely significant. This can be attributed to the low S/N ratio of these data, given that the column density of this component found in MEG and LETG are similar. We notice, however, that the O VII $K\alpha$ line is clearly detected in the data but with less significance ($\sigma \approx 2$).

5.4 Comparison between MEG and LETG models

The results from MEG and LETG are consistent. In the warm-hot component, the model over both datasets has similar column densities (within the errors) and temperatures. These parameters are strikingly similar to what has been reported in individual lines of sight (e.g., Gupta et al. 2012). Thus, our results bring more evidence to the homogeneity of this component. This is in contrast to the results found in emission, where a large dispersion up by an order of magnitude has been reported in the temperature (e.g., Henley et al. 2010; Blum

Table 2. Identified ionic absorption lines probing the super-virial hot component at $z=0$.

Ion (1)	Tran (2)	RestWav (Å) (3)	Wav (Å) (4)	EW (mÅ) (5)	$N_{\text{ion}} (\text{cm}^{-2})$ (6)	Wav (Å) (7)	EW (mÅ) (8)	$N_{\text{ion}} (\text{cm}^{-2})$ (9)	Wav (Å) (10)	EW (mÅ) (11)	EW (mÅ) (12)	$N_{\text{ion}} (\text{cm}^{-2})$ (13)	$N_{\text{ion}} (\text{cm}^{-2})$ (14)
			MEG-WARM			MEG-WARM-HOT			MEG-HOT				
			$\log(T/\text{K}) = 5.39^{+0.13}_{-0.07}$			$\log(T/\text{K}) = 6.19^{+0.06}_{-0.08}$			$\log(T/\text{K}) = 7.50 \pm 0.03$				
			$\log(N_{\text{H}}/\text{cm}^{-2}) = 18.08^{+0.31}_{-0.40}$			$\log(N_{\text{H}}/\text{cm}^{-2}) = 19.12^{+0.08}_{-0.10}$			$\log(N_{\text{H}}/\text{cm}^{-2}) = 21.30^{+0.05}_{-0.06}$				
N _{VI}	κβ	24.898	24.898	1.63	2.57×10^{15}	24.905	1.02	1.35×10^{15}					
N _{VII}	Kα	24.781				24.788	3.26	1.64×10^{15}					
Ne _{IX}	Kα	13.447				13.451	1.32	1.24×10^{15}					
O _{VII}	Kα	21.601				21.607	11.63	8.22×10^{15}					
O _{VII}	κβ	18.627				18.632	3.07	8.22×10^{15}					
O _{VII}	Kγ	17.768				17.773	1.18	8.22×10^{15}					
O _{VIII}	Kα	18.969				18.974	1.83	1.51×10^{15}	18.973	4.27		3.48×10^{15}	
S _{XVI}	Kα	4.729							4.730	0.84	$(1.07^{+0.32}_{-0.27})$	1.09×10^{16}	$(1.50^{+0.44}_{-0.38}) \times 10^{16}$
Si _{XIV}	Kα	6.182							6.184	0.93	(1.06 ± 0.20)	6.99×10^{15}	$(8.7 \pm 1.6) \times 10^{15}$
			LETG-WARM			LETG-WARM-HOT			LETG-HOT				
			$\log(T/\text{K}) = 5.64 \pm 0.06$			$\log(T/\text{K}) = 6.56 \pm 0.12$			$\log(T/\text{K}) = 7.50 \pm 0.05$				
			$\log(N_{\text{H}}/\text{cm}^{-2}) = 19.76^{+0.09}_{-0.11}$			$\log(N_{\text{H}}/\text{cm}^{-2}) = 19.56^{+0.21}_{-0.27}$			$\log(N_{\text{H}}/\text{cm}^{-2}) = 21.75^{+0.08}_{-0.14}$				
Ne _{IX}	Kα	13.447				13.448	2.57	2.49×10^{15}					
O _{VI}	Kα	22.034	22.037	3.75	2.42×10^{15}								
O _{VII}	Kα	21.601	21.603	15.81	3.95×10^{16}	21.602	3.87	1.5×10^{15}					
O _{VIII}	Kα	18.969				18.970	6.42	6.09×10^{15}	18.984	8.51		7.03×10^{15}	
S _{XVI}	Kα	4.729							4.733	5.05	$(4.87^{+1.79}_{-1.75})$	7.83×10^{16}	$(6.80^{+2.51}_{-2.44}) \times 10^{16}$
Si _{XIV}	Kα	6.182							6.187	3.85	$(3.49^{+1.28}_{-1.30})$	3.12×10^{16}	$(2.85^{+1.05}_{-1.06}) \times 10^{16}$

et al. 2022; Gupta et al. 2023 and references therein; Bhattacharyya et al. 2023).

The same happens with the temperature of the hot component, which is consistent within the errors between the two datasets. However, there is a factor of ~ 3 in the column densities between the data of the two instruments. We note that only one source in LETG is not present in MEG stacked spectrum. Nevertheless, there are 38 more sources in MEG than in LETG. Therefore, this result, along with the consistency between our findings and those found in individual lines of sight (Das et al. 2019a, Das et al. 2021b), suggest that this component might also be homogeneous in temperature but with some dispersion in column density.

In the warm component, there are some differences between MEG and LETG. These differences are marginal in temperature but become much larger in terms of column density. We find that this component is only constrained through one or two lines from one or two ions. Given this, and the low S/N ratio in the LETG data, and the low significance of this component in the MEG data, we consider that while we have enough evidence for the presence of this component (e.g., Tumlinson et al. 2017), we cannot constrain robustly its parameters.

5.5 Atomic abundances in the hot component

We find additional evidence of inhomogeneities in the hot component in addition to those in the column density reported above. In particular, the abundance of S_{XVI} is ~ 3.5 times larger in LETG than in MEG. Additionally, we find that Si/O in LETG is ~ 2 times that in MEG. The abundance of Fe is strikingly below what is expected for solar mixture. As observed in Figure 3, this is a strong observational constraint. In LETG we required O/Fe larger than solar by at least a factor of 6, and in MEG by at least a factor of 4. The sub-solar Fe/O was also found by Das et al. (2019a) and Das et al. (2021b). Abundances for other atoms are consistent with solar mixture, but we notice that the sensitivity of both stacked spectra is very limited for many of the absorption transitions.

These results, along with other claims of the non-solar mixture in the hot component (e.g., for Ne/O Das et al. 2019a, Das et al.

2021b, Gupta et al. 2021; for Si/O Das et al. 2021b) suggest that it has inhomogeneous element abundance mixtures which are different than solar.

5.6 Dispersion Measure of the hot phase

In the present work, the column density of the hot phase as measured in MEG data is

$$N_{\text{H}} = 2 \times 10^{21} \text{cm}^{-2} \left(\frac{A_{\text{O}}/A_{\text{H}}}{4.9 \times 10^{-4}} \right)^{-1} \left(\frac{Z/Z_{\odot}}{1} \right)^{-1}, \quad (1)$$

where the Oxygen abundance ($A_{\text{O}}/A_{\text{H}}$) and metallicity (Z) in the PHASE models discussed in this paper have been assumed to be solar ($A_{\text{O}}/A_{\text{H}} = 4.9 \times 10^{-4}$ Asplund et al. (2009) and $Z = 1Z_{\odot}$). The dispersion measure (DM), however, provides a constraint on the combination of these parameters.

The DM of the CGM has been investigated using Fast Radio Bursts (FRBs) and Galactic Pulsars (e.g., Prochaska & Zheng 2019; Platts et al. 2020; Das et al. 2021a; Cook et al. 2023). Platts et al. 2020 found a DM for the Galactic halo (DM_{total}) of

$$DM_{\text{total}} = 63^{+27}_{-21} \text{pc cm}^{-3}, \quad (2)$$

where the errors are 1σ .

We calculated the contribution to the DM from the warm-hot component (DM_{virial}) using equation (5) from Das et al. (2021a). By considering the O_{VII} column density ($N_{\text{OVII}} = 8.22^{+2.8}_{-2.97} \times 10^{15} \text{cm}^{-2}$) and its ionic fraction (0.826) on the MEG-WARM-HOT component, we obtained $DM_{\text{virial}} = 7.9^{+2.8}_{-2.9} \text{cm}^{-3} \text{pc}$. We then calculated the DM for the super-virial component using

$$DM_{\text{super-virial}} = DM_{\text{total}} - DM_{\text{virial}}. \quad (3)$$

This results in $DM_{\text{super-virial}} = 55.1^{+29.9}_{-23.7} \text{pc cm}^{-3}$. Therefore, for satisfying Eq 1 and Eq 3 at the same time, $\left(\frac{A_{\text{O}}}{A_{\text{H}}} \right) \left(\frac{Z}{Z_{\odot}} \right) = 4.48^{+3.40}_{-1.57} \times 10^{-3}$ is required.

These results implies that the observed hot gas is either enriched in Oxygen, Silicon and Sulfur (the elements driving the detection of the `hot` component in this work), or has super-solar metallicity or a combination of both. For the best value of $DM_{\text{super-virial}} = 55.1 \text{ pc cm}^{-3}$, and assuming solar abundance, the metallicity required would be ~ 9 times solar, or over 6 solar assuming the 1σ lower limit. In § 5.5 we already discussed the over solar mixture of these elements. This further suggests that the hot component finds its origin in galactic winds of enriched material.

5.7 Contribution for $\text{O}_{\text{II}} \text{K}\beta$?

Finally, we note that the rest wavelength of $\text{O}_{\text{VI}} \text{K}\alpha$ is 22.034 Å. This wavelength also corresponds to the rest-wavelength of $\text{O}_{\text{II}} \text{K}\beta$ (22.04 Å; Mathur et al. 2017). We are uncertain about the contribution of $\text{O}_{\text{II}} \text{K}\beta$ to the $\text{O}_{\text{VI}} \text{K}\alpha$ absorption line. However, this possible contamination by O_{II} does not affect the detection of the `warm` component since $\text{N}_{\text{VI}} \text{K}\beta$ in MEG (EW = 1.63 mÅ), arising from this gas, is detected.

6 CONCLUSION

Our detections confirm the presence of the `hot` component of the Milky Way's CGM coexisting with a `warm` and `warm-hot` phases. The characteristic high temperature at $\log(T/\text{K}) \sim 7.5$ of this component where Si_{XIV} and S_{XVI} are detected is further supported by the non-detection of Ne_{X} , since Ne is expected to be almost completely ionized into Ne_{X} at those temperatures, and its abundance is not that high as that for Oxygen. This result also excludes the presence of high quantities of gas in the CGM with temperatures $\log(T/\text{K})$ over ~ 6.5 and below ~ 7.5 . This `hot` component is permeating the Milky Way's CGM, and points to be homogeneous in temperature and inhomogeneous in column density.

In our analysis of Lara-DI et al. 2023, we inspected for each sightline the presence of prominent absorption lines at $z = 0$. None of these individual sightlines present these prominent features. Moreover, we conducted simulations to evaluate whether the observed detections could arise from only a few sightlines. We determined the likelihood of encountering, in an N-sightlines stacked spectrum, individual spectra presenting an absorption line at least N times stronger than that detected in the stacked spectrum. Our analysis indicates that after stacking 40 spectra, this probability diminishes to a negligible value. Therefore, our results point to a hot phase being widespread in the halo - since the final stacked spectra is the result of the contribution from many sightlines.

In order to be consistent with the DM obtained from FRBs in the literature, the hot CGM gas observed in the halo is either enriched in Oxygen, Silicon, and Sulfur, or has metallicity of at least 4.4 times solar value, or a combination of both. This, along with the sub-solar Fe/O found for this component, and that found in the ISM in other works, are key for understanding the heating, cooling and mixing mechanisms within the CGM. In particular, our results provide tantalizing suggestions that the super-virial component of the CGM is the result of feedback from winds arising in the Galaxy.

ACKNOWLEDGMENTS

The authors of this work thank the anonymous referee for his/her valuable comments. L.D.I. acknowledges support from CONACYT

through the PhD scholarship grant 760672. Y.K. acknowledges support from grant DGAPA PAPIIT 102023. S.M. is grateful for the grant provided by the National Aeronautics and Space Administration through Chandra Award Number AR0-21016X issued by the Chandra X-ray Center, which is operated by the Smithsonian Astrophysical Observatory for and on behalf of the National Aeronautics Space Administration under contract NAS8-03060. S.M. is also grateful for the NASA ADAP grant 80NSSC22K1121. S.D. acknowledges support from the KIPAC Fellowship of Kavli Institute for Particle Astrophysics and Cosmology Stanford University.

DATA AVAILABILITY

All data used in this article are available online via the Chandra Data Archive: <https://cda.harvard.edu/chaser/>

REFERENCES

- Asplund M., Grevesse N., Sauval A. J., Scott P., 2009, *ARA&A*, 47, 481
- Bhattacharyya J., Das S., Gupta A., Mathur S., Krongold Y., 2023, *ApJ*, 952, 41
- Bluem J., et al., 2022, *ApJ*, 936, 72
- Cook A. M., et al., 2023, *The Astrophysical Journal*, 946, 58
- Das S., Mathur S., Nicastro F., Krongold Y., 2019a, *ApJ*, 882, L23
- Das S., Mathur S., Gupta A., Nicastro F., Krongold Y., 2019b, *The Astrophysical Journal*, 887, 257
- Das S., Mathur S., Gupta A., Nicastro F., Krongold Y., 2021a, *MNRAS*, 500, 655
- Das S., Mathur S., Gupta A., Krongold Y., 2021b, *ApJ*, 918, 83
- Feldmann R., Hooper D., Gnedin N. Y., 2013, *ApJ*, 763, 21
- Gupta A., Mathur S., Krongold Y., Nicastro F., Galeazzi M., 2012, *ApJ*, 756, L8
- Gupta A., Kingsbury J., Mathur S., Das S., Galeazzi M., Krongold Y., Nicastro F., 2021, *ApJ*, 909, 164
- Gupta A., Mathur S., Kingsbury J., Das S., Krongold Y., 2023, in *AAS/High Energy Astrophysics Division*. p. 102.19
- Henley D. B., Shelton R. L., Kwak K., Joung M. R., Low M.-M. M., 2010, *The Astrophysical Journal*, 723, 935
- Kereš D., Katz N., Weinberg D. H., Davé R., 2005, *Monthly Notices of the Royal Astronomical Society*, 363, 2
- Kirkman D., Tytler D., Suzuki N., O'Meara J. M., Lubin D., 2003, *ApJS*, 149, 1
- Krongold Y., Nicastro F., Brickhouse N. S., Elvis M., Liedahl D. A., Mathur S., 2003, *ApJ*, 597, 832
- Krongold Y., Nicastro F., Elvis M., Brickhouse N., Binette L., Mathur S., Jiménez-Bailón E., 2007, *ApJ*, 659, 1022
- Lara-DI A., Mathur S., Krongold Y., Das S., Gupta A., 2023, *The Astrophysical Journal*, 946, 55
- Li J.-T., Bregman J. N., Wang Q. D., Crain R. A., Anderson M. E., 2018, *The Astrophysical Journal Letters*, 855, L24
- Mathur S., 2022, *Probing the Circumgalactic Medium with X-Ray Absorption Lines*. Springer Nature Singapore, Singapore, pp 1–36, doi:10.1007/978-981-16-4544-0_112-1, https://doi.org/10.1007/978-981-16-4544-0_112-1
- Mathur S., Nicastro F., Gupta A., Krongold Y., McLaughlin B. M., Brickhouse N., Pradhan A., 2017, *ApJ*, 851, L7
- Mathur S., Gupta A., Das S., Krongold Y., Nicastro F., 2021, *ApJ*, 908, 69
- Mathur S., Das S., Gupta A., Krongold Y., 2023, *Monthly Notices of the Royal Astronomical Society: Letters*, 525, L11
- McClain R. L., Mathur S., Das S., Krongold Y., Gupta A., 2024, *MNRAS*, 527, 5093
- McGaugh S. S., Schombert J. M., de Blok W. J. G., Zagursky M. J., 2010, *ApJ*, 708, L14
- Peebles M. S., Werk J. K., Tumlinson J., Oppenheimer B. D., Prochaska J. X., Katz N., Weinberg D. H., 2014, *ApJ*, 786, 54

- Planck Collaboration et al., 2016, *A&A*, 594, A13
Platts E., Prochaska J. X., Law C. J., 2020, *ApJ*, 895, L49
Prochaska J. X., Zheng Y., 2019, *Monthly Notices of the Royal Astronomical Society*, 485, 648
Stinson G. S., et al., 2012, *MNRAS*, 425, 1270
Tumlinson J., Peebles M. S., Werk J. K., 2017, *ARA&A*, 55, 389
Wang Q. D., et al., 2005, *The Astrophysical Journal*, 635, 386
Zheng Y., Putman M. E., Peek J. E. G., Joung M. R., 2015, *ApJ*, 807, 103

This paper has been typeset from a $\text{\TeX}/\text{\LaTeX}$ file prepared by the author.